 doi:10.20944/preprints201608.0206.v2

Article

Short-Range Vital Signs Sensing Based on EEMD and CWT Using IR-UWB Radar

Xikun Hu and Tian Jin *

College of Electronic Science and Engineering, National University of Defense Technology, Changsha 410073, China; xikung_hu@126.com; tianjin@nudt.edu.cn

* Correspondence: tianjin@nudt.edu.cn

Abstract: The radar sensor described realizes healthcare monitoring capable of detecting subject chest-wall movement caused by cardiopulmonary activities, and wirelessly estimating the respiration and heartbeat rates of the subject without attaching any devices to the body. No conventional Doppler only can capture Doppler signatures because of a lack of bandwidth information with noncontact sensors. In contrast, we take full advantages of impulse radio ultra-wideband (IR-UWB) radar to achieve low power consumption and convenient portability, with a flexible detection range and desirable accuracy. A noise reduction method based on improved ensemble empirical mode decomposition (EEMD) and a vital sign separation method based on continuous-wavelet transform (CWT) are proposed jointly to improve the signal-to-noise ratio (SNR) in order to acquire accurate respiration and heartbeat rates. This noncontact healthcare sensor system proves the commercial feasibility and considerable accessibility of using compact IR-UWB radar for emerging biomedical applications. Compared with traditional contact measurement devices, experimental results utilizing a 2.3 GHz bandwidth transceiver, demonstrate 100% similar results.

Keywords: impulse radio ultra-wideband (IR-UWB) radar; noncontact; short-range; vital signs; ensemble empirical mode decomposition (EEMD); continuous-wavelet transform (CWT)

---

1. Introduction

Radar sensors have been widely used in a number of applications since the 1930s [1], from primary vehicle speed measurement to advanced air-defense and marine radars, all of which are usually developed for ranging, targeting, or tracking moving subjects at large distances. Due to its noninvasive and noncontact properties, short-range radar has been an appealing approach in healthcare applications since the 1970s, when the first short-range non-invasive radar for respiration measurement was introduced [2]. Based on the principle of electromagnetic backscattering [3], radar is capable of wirelessly detecting both chest-wall movements caused by respiration and extremely small heart beats. Conventional medical devices like an electrocardiograph (ECG) and respiration belt rely on electrodes alone and an inductive plethysmograph, respectively, which make subjects uncomfortable, and may even worsen the quality of physiological measurements. In long-term monitoring (i.e., for obstructive sleep / coma subjects), an alarm connected to a radar processor can be triggered to either wake the subject or send a message to the subject's nursing assistants so that they can take measures immediately to avoid possible danger or accidents [4]. In contrast, wearable devices require that the subject be attached to electric poles twisted together with several wires for heartbeat monitoring or a vacuum belt for respiratory monitoring during sleep, which may have a negative impact on sleep quality [5].

Ultra-wideband (UWB) radar is a technology used for transmitting electromagnetic waves spread over a large bandwidth (normally larger than 500MHz). Typically, most UWB radars transmit via large bandwidth over short pulse periods, usually on the order of a nanosecond, or even a picosecond; we generally refer to this type of UWB signalling as impulse radio UWB (IR-UWB) radar [6-8]. This has gained popularity in social and military applications in through-wall imaging, ground penetrating radar, detection of moving targets, and so on owing to its high penetrability and high range resolution [9]. These characteristics make IR-UWB radar attractive for noncontact vital sign detection because it is capable of measuring absolute distance while carrying more vital sign information [10-13]. Other than IR-UWB radar, continuous-wave (CW) radar is a basic type of radar used to detect phase information related to Doppler shift due to a moving chest wall. CW radar falls into three subcategories basically: single-tone, stepped frequency CW (SFCW), and frequency-modulated CW (FMCW) [14]. Each type of radar has its specific advantages. Single-tone CW radar also has a simple system architecture considering high-level chip integration [15,16], though it carries no absolute distance information. On the other hand, FMCW radars can obtain range information [17] but normally require quite a large bandwidth and more sophisticated signal processing to realize accurate relative displacement measurements. Comprehensively taking the complexity of signal processing and power consumption into consideration, IR-UWB radar seems to be a better option for further applications. In addition, with the advancement of system integration chip technologies, nano-scale UWB impulse radar transceiver chips have been developed in recent years, realizing superfast sampling rate reaching around 39 GS/s with low-power consumption [18], which makes them more attractive for mobile, portable, and even handheld applications in future trends.

Since the 21st century, significant research has been performed on noncontact monitoring of vital signs of a subject through IR-UWB radar systems [19-26]. In [23] the mathematical modelling of the received waveforms was presented considering the magnitudes of different breathing harmonics and intermodulation, and then non-invasive monitoring of breathing and heartbeat rates was realized using an independent complex generator and sampler, which inevitably made the system heavy. To decrease the weight of the radar system, Khan et al. made it feasible to monitor the vital signs of a non-stationary human using an IR-UWB transceiver chip, but this work did not optimize the complete implementation procedures from the signal mathematical model to the experimental results under practical scenarios [24]. Moreover, Huang et al. utilized another kind of UWB radar to monitor infant respiration, but made no reference to heartbeat detection [25]. Typically, in relaxed human beings, the heart can experience heart displacements of 0.6 mm and respiration displacements are between 12 mm and several centimeters, depending on the person [26]. However, the spectrum of the detected signal contains several harmonics of the breathing signal that can be much stronger than the frequency component of the heartbeat signal [23]. Therefore, it is much more difficult to extract heartbeat signals from complicated radar echo signals. In this paper, the breathing rate and heartbeat frequency are detected remotely and are separated based on a one time-frequency analysis method which combines ensemble empirical mode decomposition (EEMD) with continuous-wavelet transform (CWT). The proposed method can increase the signal-to-noise ratio (SNR) to a certain degree compared with the traditional filtering method [11].

The remainder of this paper is organized as follows. Section 2 presents a mathematical model of vital signs. The signal processing techniques used to detect the respiration and heart rates are presented in Section 3. We describe the proposed IR-UWB sensor system and the experimental setup in Section 4. In Section 5, Experimental results and comparisons are presented. Section 6 concludes this paper.

2. Mathematical Model of Vital Sign

By observing the changes in the propagating time delay of the echo signal from a subject, we can detect the range remotely. When the transmitted pulse illuminates a human subject, part of it is reflected back to the radar because of the high reflectivity of the body [19].

For further digital signal processing, the received waveforms are measured at discrete instants in slow-time $t = nT_s$ $(n = 0,1, \dots N-1)$, where T_s is the effective pulse repetition time and N discrete-time sequences are stored after the received signal is sampled. In fast time, τ is the propagation fast-time of the electromagnetic wave. T_f is the sampling period in fast-time, and $m = 0,1, \dots, M-1$ are the fast-time sampling points. Let $s(t)$ represent the transmitted signal. The discrete signal can be expressed as an $M \times N$ matrix $\boldsymbol{R}$, the elements of which are [23]:

$$R[n,m] = \sum_i a_i s\left(mT_f - \tau_i\right) + a_v s\left(mT_f - \tau_v\left(nT_s\right)\right), \tag{1}$$

where a_i and τ_i are the amplitude and propagation time delay of static target i in fast-time and a_v is the amplitude. $\tau_v(t)$ is the propagation time delay of object reflection in fast-time.

In a static environment, the clutter can be considered as a DC-component in the slow-time direction. From (1) it is clear that background clutter does not depend on slow-time t. Thus, we can use basic filter to remove the background clutter, which can be done easily by subtracting the mean from the matrix $\boldsymbol{R}$ [23]. Let $r(t,\tau)$ represent the received signal; then the signal after clutter suppression can be expressed as:

$$x(t,\tau) = a_v s(\tau - \tau_v(t)) - r_0(\tau) = r(t,\tau) - \lim_{T\to\infty} \frac{1}{T}\int_0^T r(t,\tau)dt\,. \tag{2}$$

The DC component $r_0(\tau)$ is blocked by subtracting the average of all samples in fast-time.

According to (2) we can obtain the ideal signal without any stationary background as below:

$$y(t,\tau) = a_v s(\tau - \tau_v(t)) = a_v s(\tau - \tau_0 - \tau_r \sin(2\pi f_r t) + \tau_h \sin(2\pi f_h t))\,. \tag{3}$$

In order to estimate the respiratory frequency f_r and heartbeat frequency f_h, the Fourier transform of (3) is performed in slow-time:

$$Y(f,\tau) = \int_{-\infty}^{+\infty} Y(f,v) e^{j2\pi ft} dv,. \tag{4}$$

After simplifying using the Bessel series [21], the spectrum in slow-time is expressed as below:

$$Y(f,\tau) = a_v \sum_{k=-\infty}^{+\infty} \sum_{l=-\infty}^{+\infty} G_{kl} \delta(f - kf_r - lf_h)\,. \tag{5}$$

It is clear from (5) that the spectrum of the signal in the slow-time index is a discrete function which consists of the respiratory rate f_r, heartbeat rate f_h and a train of harmonics. The amplitude G_{kl} is related to the fast-time, and it controls the amplitude of each intermodulation product for a frequency of $f = kf_r + lf_h$.

3. Detection Algorithm

In this section, we propose and elaborate on the detection method combining noise reduction method based on EEMD with a separation method based on the CWT for impulse UWB signal modules.

Facing the problems of moving interference from the environment, the combined methods are proposed in [27], which include several ordinary methods of extracting periodic signal from noise such as using an adaptive line enhancer (ALE), blind source separation, empirical mode decomposition (EMD), *etc.*, and [27] concludes that the effect is not obvious when using one method of the mentioned methods. In sensing a human subject outdoors in [27], it is necessary to remove interference continuously, so ALE is added to reduce the Gaussian noise signal of the detected respiration adaptively. However, for the remotely sensing of vital signs including not only respiration but also heartbeat, higher SNR improvement is required. Therefore, EEMD is introduced to improve the SNR, and then, after denoising, a separation algorithm based on CWT is proposed for extracting weak heartbeat signals from echo signals. Figure 1 shows the signal processing block diagram.

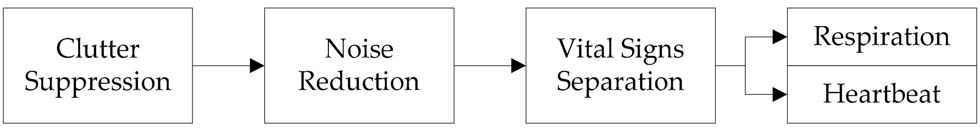

Figure 1. Flowchart of the proposed detection method.

Generally, a finite impulse response (FIR) filter can be used for cancelling noise and passing a given frequency bandwidth. Since the amplitude of respiration is much larger than that of a heartbeat, it is easy to observe periodic waves from the baseband output [11]. Therefore, a traditional processing method using a band-pass FIR filter to separate the vital signs is introduced as showed in Figure 2. According to prior knowledge that the normal heartbeat rate varies from 60 to 100 beats/min (about 1.0–1.6 Hz), in order to obtain the heartbeat signal, the frequency window is set to be 0.65–3.0 Hz. To reject out-of-band noise and to obtain the respiration signal, a low-pass elliptic FIR filter is applied. Comparative experiments between the proposed method and the traditional FIR filtering method are presented in Section 5.1.

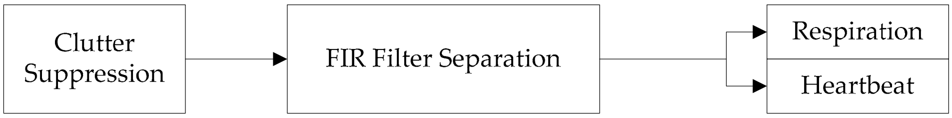

Figure 2. Traditional FIR filtering method.

3.1. Clutter Suppression Algorithm

In a static environment, the clutter from the background can be considered as DC component and can be removed easily by subtracting the mean from the matrix $\boldsymbol{R}\,[\boldsymbol{n},\boldsymbol{m}]$ in (1) in both rows and columns. To suppress the background of a stationary target and the antenna crosstalk effect, summing and averaging amplitudes along fast-time range bins identifies the strength of the clutter, and owing to periodic amplitude cancellation, $x(t,\tau)$ contains little information about vital signs. This is simplified by referring to $x_{m,n}$, denoting the n-th slow-time sample of the m-th range bins. In the fast-time domain, the detection range is divided into M bins. To obtain the position of the target, the ideal number of range bins is calculated as described below:

$$v = \arg\max_{m}\left(\sum_{n=1}^{N}\left(x_{m,n} - \frac{1}{N}\sum_{n=1}^{N} x_{m,n}\right)^{2}\right), \tag{6}$$

where $n = 0,1,\dots N-1$ represents the number of pulses, and $m = 0,1,\dots,M-1$ is the number of range bins in fast-time. v denotes the selected vital signs bin between 0-*M-1*. Finally, the slow-time signal $x_{v,n}$ is the vital sign signal we require.

3.2. Noise Reduction Method Based on Improved EEMD Algorithm

The purpose of the EMD procedure is to decompose the time series into a superposition of its intrinsic sub-signals (mode function) with well-defined instantaneous frequencies, which are called intrinsic mode functions (IMFs).

$$x(t) = \sum_{i=1}^{n} c_i + r_n, \tag{7}$$

where $c_i, i = 1,\dots,N$ denotes N IMFs and r_n denotes the residue. An IMF is a function that satisfies two conditions: (i) the number of extrema and the number of zero crossing must be equal or differ at most by one; (ii) the mean value of the upper and lower envelopes is zero everywhere. Each of the IMFs represents the oscillation mode present in the data set with different time scale properties. The number of extrema in each IMF is decreased as the IMF order increases and the corresponding spectral supports are decreased accordingly [28]. Each IMF is estimated with an iterative process called sifting. The sifting process consists of five major steps as follows [29]:

1. The maxima and minima of signal $x(t)$ are identified.
2. The upper and lower envelops are obtained respectively by interpolating the set of maximal and minimal points using cubic spines.
3. Computing the mean of the two envelops the mean is designated as m_1 then subtraction of the mean from the original signal yields $h_1 = x(t) - m_1$, where h_1 is the first component presenting difference between the signal $x(t)$ and m_1.
4. Verifying whether or not h_1 satisfies the conditions for being an IMF. If h_1 is not the first IMF, treating h_1 as the original signal $x(t)$, steps 1-3 are repeated to yield mean m_{11} and $h_{11} = x(t) - m_{11}$, testing whether or not h_{11} satisfies the two conditions for being an IMF again, if h_{11} is not

 doi:10.20944/preprints201608.0206.v2

an IMF, steps 1-3 are repeated k times to yield mean m_{1k} and $h_{1k} = x(t) - m_{1k}$ until h_{1k} satisfies the two conditions. The first IMF $c_1 = h_{1k}$ is generated.

5. Subtraction of the c_1 from the original signal to yield $r_1 = x(t) - c_1$, where r_1 is the residue, treating r_1 as the original signal $x(t)$, steps 1-4 are repeated to yield the second IMF c_2; repeating this step, the rest of the IMFs of the original signal $x(t)$ are generated, this process can be represented by the following formula:

$$\begin{aligned} r_1 - c_2 &= r_2 \\ r_2 - c_3 &= r_3 \\ &\vdots \\ r_{n-1} - c_n &= r_n \end{aligned} \quad . \tag{8}$$

In 2011, a variation of the EEMD algorithm was proposed that provides an exact reconstruction of the original signal and a better spectral separation of the modes, with a lower computational cost [30]. Regarding EEMD [31], it defines the "true" IMF components (notated as $\widetilde{IMF}$ henceforth) as the means of the corresponding IMFs obtained via EMD over an ensemble of trials generated by adding different realizations of white noise of finite variance to the vital sign signal. Taking full advantage of the IMF components, the improved method used to reduce noise based on the improved EEMD algorithm is shown in Figure 3.

After denoising, the echo signal $x[n] = x_{v,n}$ obtained by (6) can be rewritten for the n-th slow-time:

$$x[n] = \sum_{k=1}^{K} \widetilde{IMF}_k , \tag{9}$$

without the residue; on the other hand, we can choose several (not all) of the $\widetilde{IMF}$s from $k = 1, \dots, K$ to reconstruct out ideal echo signal.

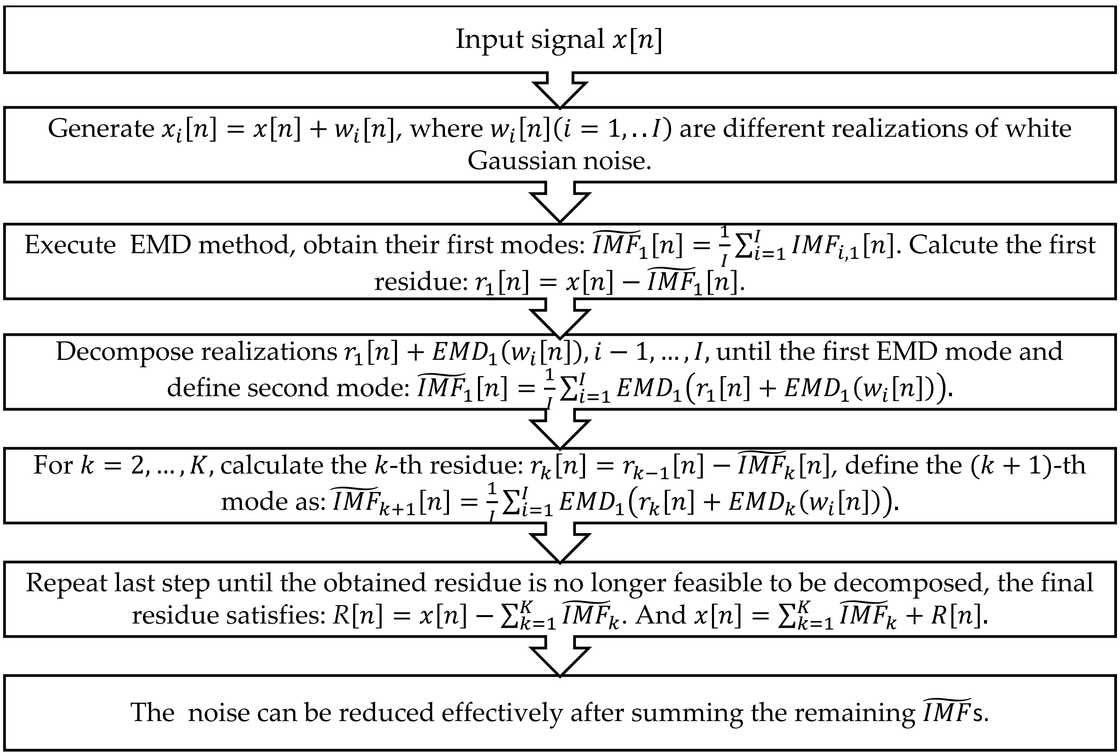

Figure 3. Noise reduction method based on improved EEMD algorithm [28].

3.3. Separation Method Based on the Continuous-Wavelet Transform

First, we introduce the signal analysis methods, from the frequency analysis method of Fourier transform (FT) to time-frequency methods like the short time Fourier transform (STFT) and CWT, all

Preprints (www.preprints.org) | NOT PEER-REVIEWED | Posted: 15 September 2016 doi:10.20944/preprints201608.0206.v2

of which are variations of the FT. Like the FT, the CWT uses inner products to measure the similarity between a signal and an analysis function. In the FT, the analysing functions are complex exponentials $e^{-j\omega t}$. The resulting transform is a function of a single variable, ω. In the STFT, the analysis functions are windowed complex exponentials, $w(t)e^{j\omega t}$, and the result is a function of two variables. The STFT coefficients, $F(\omega,\tau)$, represent the match between the signal and a sinusoid with angular frequency ω in an interval of a specified length centred at τ. In the CWT, the analysis function is a wavelet, ψ. The CWT compares the signal to shifted and compressed or stretched versions of a wavelet. Stretching or compressing a function is collectively referred to as dilation or scaling and corresponds to the physical notion of scale. By comparing the signal to the wavelet at various scales and positions, we obtain a function of two variables. If the wavelet is complex-valued, the CWT is a complex-valued function of scale and position. If the signal is real-valued, the CWT is a real-valued function of scale and position. For a scale parameter, $a > 0$, and position, b, the CWT of signal $f(t)$ is:

$$C(a,b;f(t),\psi(t)) = \int_{-\infty}^{\infty} f(t)\frac{1}{\sqrt{a}}\psi^*(\frac{t-b}{a})dt, \tag{10}$$

where $*$ denotes the complex conjugate. Not only do the values of scale and position affect the CWT coefficients; the choice of wavelet also affects the values of the coefficients.

After denoising, it is very difficult to extract a heartbeat signal from an echo signal owing to the overlap of dominated respiration amplitude. CWTs are used because of their ability to find the energy of the desired frequency interval. Wavelets provide excellent time resolution for rapid events such as heartbeats and good frequency resolution for slower events such as respiration.

The Morlet wavelet [32] is chosen as the mother wavelet to detect the frequencies in received denoised signals and then estimate the amplitude at each detected frequency. The Morlet wavelet is the most frequently used in practice because its simple numerical implementation and because the vanishing of the third-order differentiation of its phase can also simplify the computation [33]. The wavelet transform of a signal $f(x)$ with respect to a mother wavelet $g(t)$ is

$$S(\tau,a,f(t),\psi(t)) = \frac{1}{2\pi}\sqrt{a}\int F(w)G^*(aw)e^{iw\tau}dw, \tag{11}$$

where $F(w)$ is the Fourier transform of the signal, $a > 0$ is a scale parameter, $\tau \in \mathbf{R}$ is a translation parameter and $G^*(w)$ is the complex conjugate of the Fourier transform of $g(t)$. Given the spectrum of an ideal vital sign signal $f(x)$, namely $Y(f,\tau)$ in (5), the simplified expression is

$$F(w) = 2\pi\sum_{k=-\infty}^{+\infty}\sum_{l=-\infty}^{+\infty} G_{kl}\delta(w-kw_r-lw_h). \tag{12}$$

The Morlet wavelet transform of $f(x)$ is

$$\begin{aligned} S(\tau,a) &= \sqrt{a}f(\tau)\sum_{k=-\infty}^{+\infty}\sum_{l=-\infty}^{+\infty} G_{kl}G_M^*(a(kw_r+lw_h)) \\ &= \sqrt{a}f(\tau)\sum_{k=-\infty}^{+\infty}\sum_{l=-\infty}^{+\infty} G_{kl}G_M^*(a_rw_r+a_hw_h)) \end{aligned} \tag{13}$$

where

$$\begin{aligned} g_M(t) &= \frac{1}{2\pi\sigma}e^{-\frac{1}{2\sigma^2}t^2}e^{iw_0t}+\varepsilon(t) \\ G_M(w) &= e^{-\frac{\sigma^2(w-w_0)^2}{2}}+\varepsilon^*(w) \end{aligned} \tag{14}$$

is the Morlet wavelet whose frequency and width are denoted by the centre frequency of the mother wavelet w_0 and σ. From [34], the instantaneous frequency on the scale a of the Morlet transform is w_r and w_h.

$$a_r = \frac{w_0 w_s}{w_r}$$
$$a_h = \frac{w_0 w_s}{w_h} \tag{15}$$

where w_s denotes the sampling frequency. The frame size of the input signal must be a multiple of 2^n, where n is the number of levels. Using this dyadic scales presentation, the sampling frequency of the received signal is 65 Hz, roughly equal to the dyadic 6, representing 2^6. On the other hand, we select the dyadic representation of the center frequency as 8. For vital signs containing respiration and heartbeat components, the dyadic number of the former can be referred to as $a_r = 2^8 \times 2^6/2^{-2} = 2^{16}$, which is displayed as a coefficient of 16. Moreover, the heartbeat scales can be obtained via the same representation, but not in a constant number because of the weak amplitude and deep interference caused by noise. Therefore, we can only obtain an approximate range from scales 11 to 14, within which we can obtain the preferred coefficient 12. Therefore, there is no need to compute the wavelet transform at all scales. A rough approximation of the scales a_r and a_h may be read from the Fourier transform of the signal, or derived from a priori knowledge. Then, more precise values of a_r and a_h can be calculated iteratively using ridge extraction in [33]. The numbers of coefficients we choose may change along with the variance of breathing or heart rate according to (15).

The application of the Morlet wavelet decomposes the signal into a series of components and for each decomposition levels, the coefficients can be either set to zero or reduced in magnitude, so that a particular feature of the signal is affected upon reconstruction. The high-frequency (HF) components are used for heartbeat signal recovery and the low-frequency (LF) ones for respiration recovery. Finally, a moving average filter is applied to each signal; thus, the heartbeat and respiration signals are reconstructed. The signal processing proposed for recovering ideal signals can be summarized as in Figure 4.

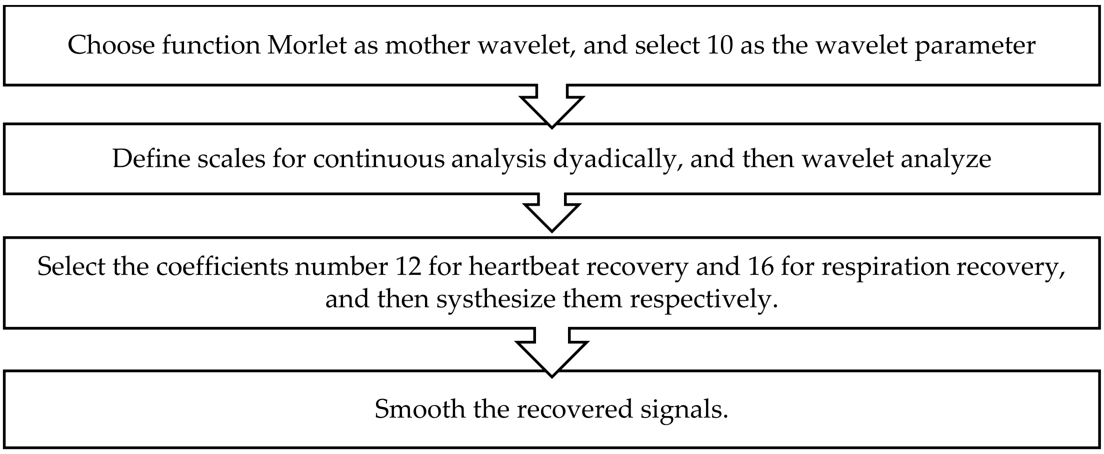

Figure 4. Flowchart of the separation method using the Morlet CWT.

4. Radar System and Experimental Setup

4.1. Radar System

The design of the sensor is based on an impulse radar NVA series 661 (Novelda, Norway) fully integrated nano-scale radar transceivers with low power consumption. It also provides flexible control of key parameters such as pulse repetition frequency (PRF), sampling rate, and samplers per frame. The chip (NVA6201) employs a novel technology called "continuous time binary value" (CTBV), which can solve some of the main problems of traditional sampling methods by excluding the demand for a high-resolution ADC while realizing the impressive time resolution of modern digital circuits. The sampling chain is realized using inherent gate-delays resulting in a rate of about

Preprints (www.preprints.org) | NOT PEER-REVIEWED | Posted: 15 September 2016 doi:10.20944/preprints201608.0206.v2

39 GS/s for a single frame, which consists of a maximum 512 samples. See for example [35] for an introduction to the implemented sampling technology.

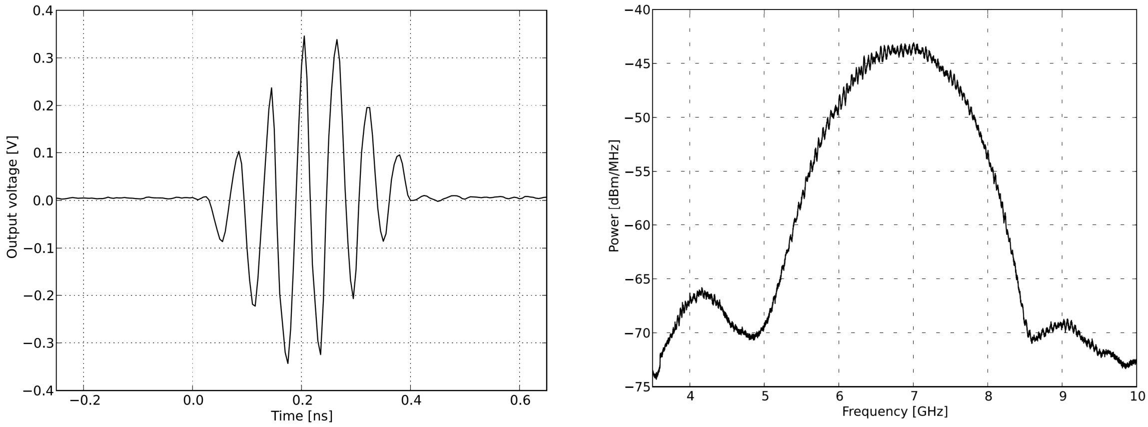

(**a**) (**b**)

Figure 5. Transmitted signal in the time domain and frequency domain. (**a**) Pulse generator time domain output; (**b**) pulse generator output spectra.

The pulse generator used to transmit the narrow Gaussian pulse signal depicted in Figure 5 (a) has a derivative of approximation of 11, with a 2.3-GHz output frequency band as showed in Figure 5 (b). After enhancement by the power amplifier, the signal is emitted by Vivaldi transmission antennas shown in Figure 6. In the receiver, the reflected echo is first received by the receiving antennas and then magnified by a low-noise amplifier (LNA). Next, the signal containing the vital sign information is sampled by a high-speed sampler with a fixed offset in sequence with a fast-time sampling frequency of about 39 GHz. Finally, the digital signal is transferred to a MATLAB processor on a computer with a slow-time frequency of about 65 Hz. The total energy consumed during one measurement is less than 120 mW [36].

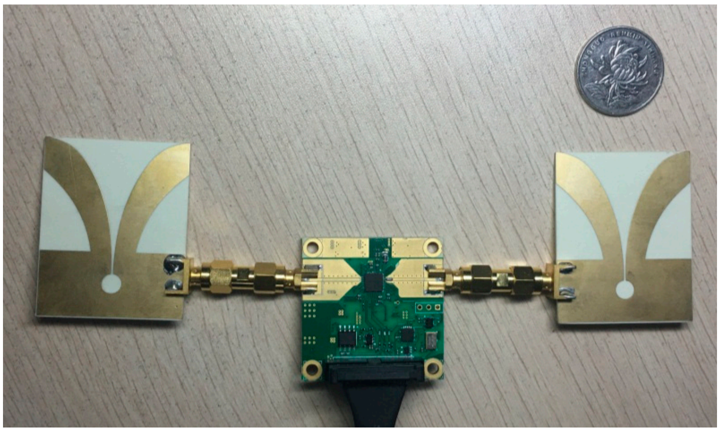

Figure 6. NVA661 nano-scale IR-UWB Radar.

4.2. Experimental Setup

Figure 7 shows the experimental setup of the radar used for measurement. The volunteer was a 22-year-old healthy male sitting in a chair and breathing regularly while medical devices simultaneously monitored him, at a distance of around 0.3 m as shown in Figure 7(a). The specifications for the measurement are given in Table 1.

In order to evaluate the performance of the radar system, we applied a comprehensive sports medicine tool (DynaMap Suite – SA7925, Thought Technology Ltd., Montreal West, Canada) as showed in Figure 7(b), as the measurement reference which can monitor several medical indices consisting of ECG, HR, IBI, and respiration, *etc.*, using BioGraph Infiniti Software to capture and export the respiratory data and ECG data.

(a)

(b)

Figure 7. Experimental setup. (**a**) Experimental scenario; (**b**) the radar sensor and DynaMap Suite.

Table 1. Specifications for the measurement.

Parameters	Specifications
Centre Frequency	6.8 GHz
Bandwidth	2.3 GHz
Distance between antennas and the target	0.3 m
Target's stance	Sitting on a chair
Power consumption	120 mW
Mean output power	-12.6 dBm
Peak-to-peak output amplitude	0.69 V

5. Results

5.1. SNR Comparison of FIR Filter and Proposed Method

Figure 8(a) refers to the original vital signs obtained after clutter suppression. From the respiration waveforms in Figures 8(b) and 8(c), it is easy to read the respiration rates since their peaks and valleys are quite obvious, but the respiration signal in Figure 8(c) has a more legible tendency and more defined signatures than that in in Figure 8(b) in the time domain. On the other hand, owing to lower reflected energy, the heartbeat waveforms in Figure 8(d) have peak-peak values of only just about 0.2 mV, and the waveform obtained using the FIR filter displays an irregular sign without any unambiguous heartbeat tendency, whereas the heartbeat waveforms in the decomposed results are stable and regular in Figure 8 (e). Above all, the proposed method works better than the traditional FIR method in sensing vital signs.

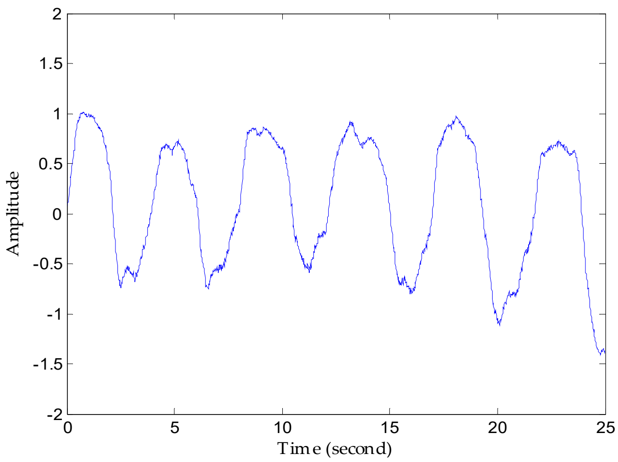

(a)

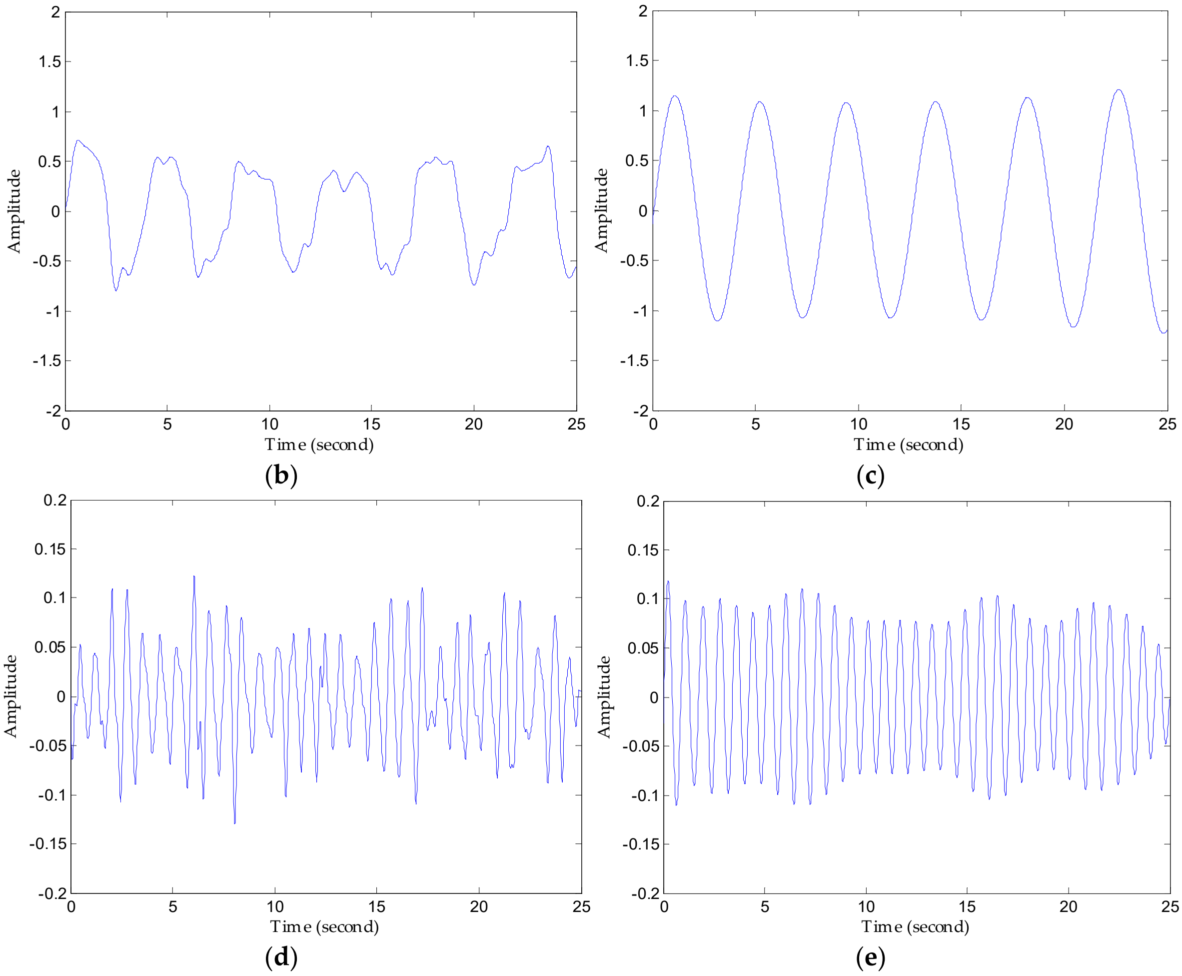

Figure 8. Comparison of results using the FIR filter and the proposed method. (**a**) The original waveforms obtained after clutter suppression; (**b**) respiration waveforms obtained via the FIR band-pass filter; (**c**) respiration waveforms obtained via the proposed method; (**d**) heartbeat waveforms obtained via the FIR band-pass filter; (**e**) heartbeat waveforms obtained via the proposed method.

The SNR criterion depends on the performance and detection precision system required, in other words, prior information can be used to determine a reasonable SNR for recognizing the respiration and heartbeat rate so reference vital signs signals are necessary to determine the unstable SNR standard. For qualitative analysis, the SNR of the vital signs signal is redefined in the frequency domain [37]. If the respiration rate is estimated as the frequency f_{max} of the peak in the frequency spectrum, the SNR is calculated as below:

$$SNR = 10\log_{10}\frac{\int_{f_{\max}-B/2}^{f_{\max}+B/2}\left|P_x(f)\right|df}{\int_0^{\infty}\left|P_x(f)\right|df-\int_{f_{\max}-B/2}^{f_{\max}+B/2}\left|P_x(f)\right|df} \tag{16}$$

where $B = 0.016$ Hz is the resolution in periodogram estimation, which is determined by the number of FFT point and the sampling frequency we demand. SNR calculations for respiration and heartbeat rates are shown in Table 2. The SNR improvement for respiration detection by the method described in this paper is 7.59 dB; moreover, the SNR improvement for heartbeat signals is 4.82 dB. Higher SNR is of vital importance for radar systems helping to decrease the false alarm probability; this is especially significantly for medical monitoring applications. In addition, higher SNR can contribute to improving detection accuracy in more complex environments, and increasing the detection range, which can help IR-UWB radar to adapt in many different environments and even to different human postures.

Preprints (www.preprints.org) | NOT PEER-REVIEWED | Posted: 15 September 2016 doi:10.20944/preprints201608.0206.v2

Table 2. SNR of respiration and heartbeat signal using FIR filter and the proposed method.

Parameters	Radar	
	FIR	Proposed Method
Respiration SNR	4.44 dB	12.03 dB
Heartbeat SNR	-53.52 dB	-48.70 dB

5.2. Detection Performance of Proposed Method

First, we denoised the signal and then separated the vital signs using the CWT method. As Figure 9 shows, it can be seen clearly from the enlarged view that the noise attached to the signal has been removed after denosing processing using an algorithm based on EEMD. Then, we used the Morlet wavelet to analyse the denoised signal and chose the 12nd scale to synthesize the respiration signal and 16th scale for the heartbeat signal effectively. The results of signal separation presented in Figure 10, from which we observe that accurate respiration signal waveforms and exact heartbeat signal waveforms can be obtained. Finally, the examples of 20 s of an extracted heartbeat signal and ECG reference signal are compared in Figure 11(a), and 120 s of an extracted respiration signal and respiration reference signal are compared in Figure 11(b).

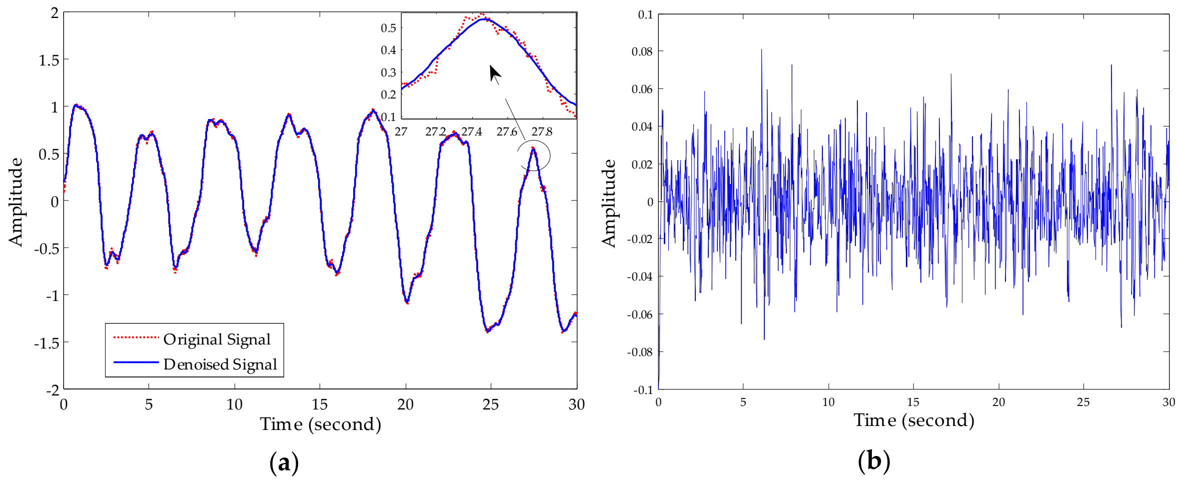

Figure 9. Performance of noise reduction. (**a**) Comparison of original vital sign signal with the denoised signal; (**b**) noise removed after denoising processing.

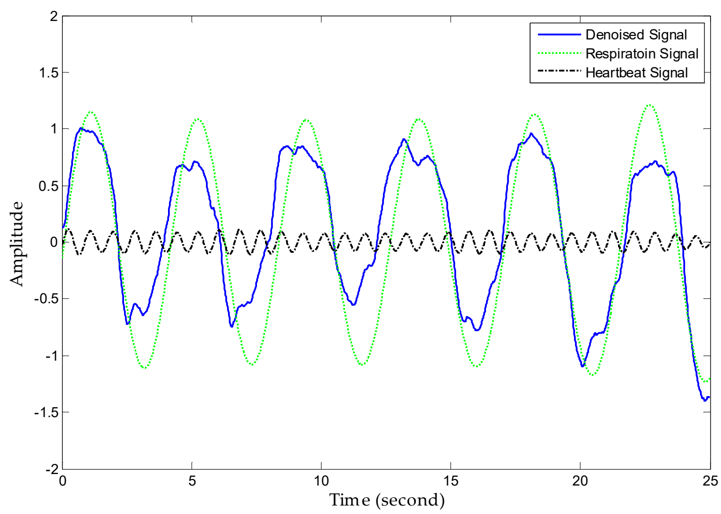

Figure 10. Performance of separation.

Preprints (www.preprints.org) | NOT PEER-REVIEWED | Posted: 15 September 2016 doi:10.20944/preprints201608.0206.v2

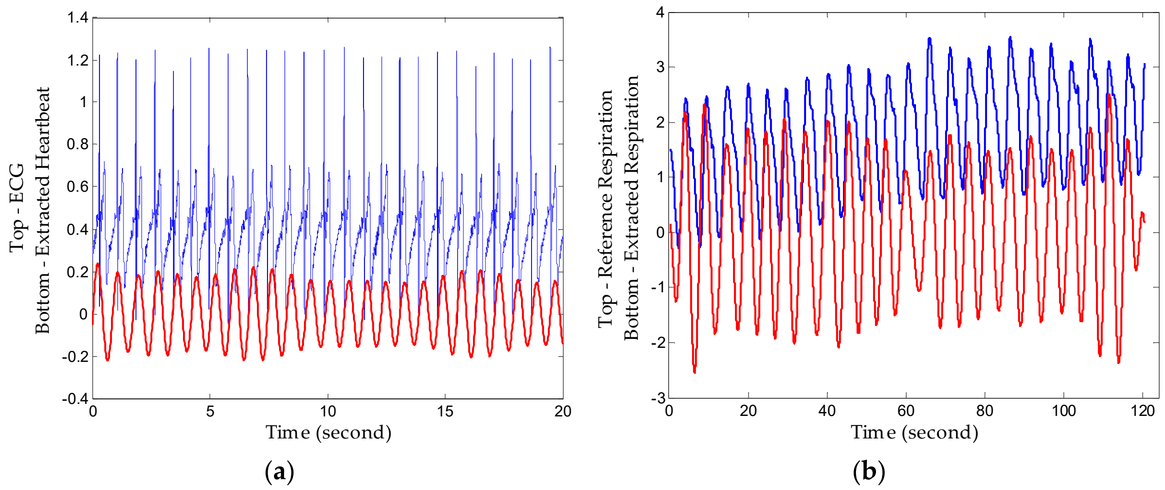

Figure 11. Extracted signals compared with reference signals. (**a**) Extracted heartbeat signal and ECG reference signal; (**b**) extracted respiration signal and respiration reference signal.

The results show that heartbeat signals superimposed on respiration signals can be decomposed with clear peaks corresponding well to the ECG, and decomposed respiration results also show a high consistency with the reference signal. Therefore, the proposed method realizes comparable detection performance to professional medical device with a high conformance to healthcare indices. Additionally, the respiration rate and heartbeat rate can be calculated simply after tracking peaks in the frequency domain or zero-crossings in time domain with low relative error since they have big amplitudes and long duration.

For further validation under various conditions, Figure 12 shows the sensor results for three subjects at 0.2-, 1.5-, and 3.0-m distances, from which the amplitudes of vital signs are seen to decrease with increasing range. Experimental results utilizing the IR-UWB radar sensor demonstrate reliable detection accuracy.

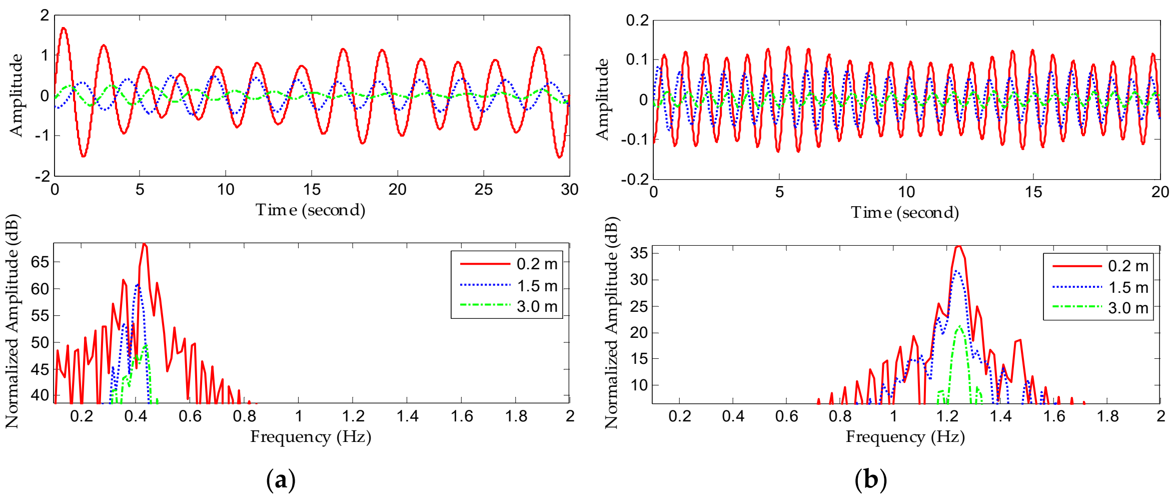

Figure 12. Detection results with different subjects at different distances. (**a**) Extracted respiration signals and frequency spectra. (**b**) Extracted heartbeat signals and frequency spectra.

6. Conclusions

This paper describes a new application of an IR-UWB radar sensor and method for non-contact detection of the vital signs of human subjects. In most previous studies, CW Doppler radar was used for detecting vital signs of human subjects within a range band carrying no absolute distance information. We applied IR-UWB technology to vital sign sensing applications, which not only eliminates the trade-off of low power consumption and system complexity versus affordable price, but also carries more vital sigh information owing to the benefit of UWB.

When the radar operates, the interferences caused by indoor targets and antennas crosstalk are common and very serious and. In this case, the SNR of an echo signal is low, which makes it difficult to extract respiration signals from complicated background noise. In order to minimize the clutter caused by environmental objects, several methods were used to improve the SNR in this study. Proposed signal processing methods involving clutter removal, denosing based on EEMD and separating based on CWT, proceeding sequentially, increase the SNR for respiration and heartbeat by 7.59 dB and 4.82 dB, respectively, compared with the traditional FIR filter method. Moreover, experimental results illustrate that respiration and heartbeat signals can be extracted well.

In future work, more biomedical parameters like HR and HRV will be tested together to check the feasibility of our proposed medical sensor system and detection methods. In addition, the influence of orientation of a non-stationary human body must be considered, which is of vital significance to long-term monitoring. Body motion noise reduction is a difficulty as noted in [38], which used two opposite radars to eliminate the effect of noise. Therefore, further work will include an improved algorithm based on the one proposed, enabling it to adjust to the non-stationary human subjects.

Acknowledgments: This work was supported by the National Natural Science Foundation of China under Grant 61271441. The authors would like to thank the Key Lab. of Medical Digital Imaging Technology, Harbin Institute of Technology Shenzhen Graduate School, for their permission to use their ECG device.

Author Contributions: Each author contributed extensively to the preparation of this manuscript. Xikun Hu developed the sensor hardware system and carried out the experiments. Tian Jin developed the algorithms. All authors participated in the discussion about the proposal and contributed to the analysis of the results.

Conflicts of Interest: The authors declare no conflict of interest. The founding sponsors had no role in the design of the study; in the collection, analyses, or interpretation of data; in the writing of the manuscript, and in the decision to publish the results.

References

1. Watson-Watt, *R. Radar in War and in Peace*. Nature 1945, 155, 319–324.
2. Lin, J.C. Non-invasive microwave measurement of respiration. IEEE Proc. 1975.
3. Skolnik, M.I. *Introduction to radar. In Radar Handbook 2*. McGraw-Hill Company: New York, NY, USA, 1962; pp. 1–18.
4. Li, C.; Lin, J.; Xiao, Y. Robust overnight monitoring of human vital signs by a non-contact respiration and heartbeat detector. In Proceedings of the 28th Annual International Conference of the IEEE, New York, NY, USA, 31 August–3 September 2006; pp. 2235–2238.
5. Yilmaz, T.; Foster, R.; Hao, Y. Detecting Vital Signs with Wearable Wireless Sensors. *Sensors* **2010**, 10, 10837–10862.
6. Cianca, E.; Gupta, B. FM-UWB for communications and radar in medical applications. *Wireless Personal Communications*. **2009**, 51, 793-809.
7. Yarovoy, A.G.; Matuzas, J.; Levitas, B.; Ligthart, P. UWB radar for human being detection. *IEEE Aero. El. Sys. Mag*. **2005**, 21, 22-26.
8. Hussain, M.G.M. Ultra-Wideband Impulse Radar: An overview of the Principles. *IEEE Aero. El. Sys. Mag*. **1998**, 13, 9-14.
9. Fontana, R.J. Recent system applications of short-pulse ultra-wideband (UWB) technology. *IEEE Trans. Microw. Theory Tech*. **2004,** 52**,** 2087-2104.
10. Xu, Y.; Dai, S.; Wu S.; Chen, J.; Fang, G. Vital Sign Detection Method Based on Multiple Higher Order Cumulant for Ultrawideband Radar. *IEEE Trans. Geosci. Remote*. **2012**, 50, 1254-1265.
11. Yan, J.; Zhao, H.; Li, Y.; Sun, L.; Hong, H.; Zhu, X. Through-the-Wall Human Respiration Detection Using Impulse Ultra-wide-band Radar. In *Biomedical Wireless* Technologies, Networks, and Sensing Systems (BioWireleSS), Proceedings of the 2016 IEEE Topical Conference, Austin, TX, USA, 24-27 January 2016; pp. 94-96.
12. McEwan, T.E. Body monitoring and imaging apparatus and method. US Patent 5.573.012. November 1996.
13. Staderini, E.M. Oral presentation: Medical applications of UWB radars. July 2008.
14. Gu, C.; Li, C. From Tumor Targeting to Speech Monitoring. *IEEE Mirco. Mag.* **2014**, 15, 66-76.

15. Li, C.; Lin, J.; Boric-Lubecke, O.; Lubecke, V. M.; Host-Madsen, A.; Park, B.-K. Development of non-contact physiological motion sensor on CMOS chip and its potential applications. In *Proc. 7th IEEE Int. Conf. Application-Specific Integrated Circuits*, Guilin, China, 26–29 Oct. 2007; pp. 1022–1027.
16. Droitcour, A. D.; Boric-Lubecke, O.; Lubecke, V. M.; Lin J. 0.25/spl mu/m CMOS and BiCMOS single-chip direct-conversion Doppler radar for remote sensing of vital signs. In *2002 IEEE Int. SolidState Circuits Conf. Tech. Dig. Papers*, 348–349.
17. Ko, H.-H.; Cheng, K.-W.; Su H.-J. Range resolution improvement for FMCW radars. In *Proc. European Radar Conf.* Oct. 2008; pp. 352–355.
18. Taylor, J.D. *Ultra-Wideband Radar Application and Design*, CRC Press, 2012, 373-387.
19. Staderini, E.M. UWB radars in medicine. *IEEE Aero. El. Sys. Mag.* **2002**, 17, 13-18.
20. Ossberger, G.; Buchegger, T.; Schimback, E.; Stelzer, A.; Weigel, R.; Non-invasive respiratory movement detection and monitoring of hidden humans using ultra wideband pulse radar. In the Proceeding of the 2004 International Workshop on Ultra Wideband Systems Joint with Conference on Ultra Wideband Systems and Technologies, Kyoto, Japan, 18-21 May 2004; pp. 395–399.
21. Venkatesh, S.; Anderson, C.; Rivera, N.V.; Buehrer, R.M. Implementation and analysis of respiration-rate estimation using impulse-based UWB. In 2005 IEEE Military Communications Conference (MILCOM 2005), 17- 20 October 2005; pp. 3314–3320.
22. Bilich, C.G. Bio-medical Sensing using Ultra Wideband Communications and Radar Technology: A Feasibility Study. In *IEEE Pervasive Health Conference and Workshops*, 19, 29 November - 01 December 2006; pp. 1-9.
23. Lazaro, A.; Girbau, D.; Villarino, R. Analysis of Vital Signs Monitoring Using an IR-UWB Radar, Progress In Electromagnetics Research, *PIER* **2010**, 100, 265-284.
24. Khan, F.; Choi, J.W.; Cho, S.H. Vital Sign Monitoring of a Non-stationary Human Through IR-UWB Radar. In Proceeding of 2014 IEEE International Conference on Network Infrastructure and Digital Content (IC-NIDC 2014), Beijing, China, 19-21 September 2014; pp. 511-514.
25. Huang, X.; Sun, L.; Tian, T.; Huang Z.; Clancy, E. Real-time noncontact infant respiratory monitoring using UWB radar. In the 16th IEEE International Conference on Communication Technology (ICCT), Hangzhou, China, 18-21 October 2015; pp.493-496.
26. Singh, M.; Ramachandran, G. Reconstruction of sequential cardiac in-plane displacement patterns on the chest wall by laser speckle interferometry. *IEEE Trans. Biomed. Eng*. **1991**, 38, 483-489.
27. Li, C.; Chen, F.; Jin, J.; Lv, H.; Li, S.; Lu, G.; Wang, J. A Method for Remotely Sensing Vital Signs of Human Subjects Outdoors. *Sensors* **2014,** 15, 14830-14844.
28. Flandrin, P.; Rilling, G.; Goncalves, P.; Empirical mode decomposition as a filter bank. *IEEE Signal Proc. Let.* **2004**, 11, 112-114.
29. Huang, N.E. et al. The Empirical Mode Decomposition and the Hilbert Spectrum for Nonlinear and Non-Stationary Time Series Analysis. *Proceedings: Mathmatical, Physical and Engineering Sciences.* **1998,** 454, 903–995.
30. Torres, M. E.; Colominas, M.A.; Schlotthauer, G.; Flandrin, P. A Complete Ensemble Empirical Mode Decomposition with Adaptive Noise. In 2011 IEEE International Conference on Accoustics, Speech and Signal Processing (ICASSP), 22-27 May 2011; pp. 4144-4147.
31. Wu, Z.; Huang, N. E. Ensemble empirical mode decomposition: A noise-assisted data analysis method. *Adv. Adapt. Data Anal*. **2009**, 01, 1–41.
32. Baboli, M.; Ghorashi, S.A.; Saniei, N.; Ahmadian, A. A New Wavelet Based Algorithm for Estimating Respiratory Motion Rate Using UWB Radar. In Proceeding of the 2009 International Conference on Biomedical and Pharmaceutical Engineering (ICBPE), Singapore, 2-4 December 2009; pp. 1-3.
33. Delprat, N.; B. Escudie, Guillemain, P.; Kronland-Martinet, R.; Tchamitchian, P.; Torresani, B. Asymptotic wavelet and Gabor analysis extraction of instantaneous frequencies. *IEEE Trans. on Inform. Theory*. **1992**, 38, 644–664.
34. Suvichakorn, A.; Antoine, J. P. Analyzing NMR spectra with the Morlet wavelet. 16th European Signal Processing Conference (EUSIPCO 2008), Lausanne, Switzerland, 25-29 August, 2008.
35. Hjortland, H.A.; Wisland, D.T.; Lande, T.S.; Limbodal, C.; Meisal, K. Thresholded Samples for UWB Impulse Radar. In *IEEE International Symposium on Circuits and Systems (ISCAS)*, 27-30 May 2007; pp. 1210-1213.
36. Novelda. NV A620x Preliminary Datasheet. Novelda, October 2013.

 doi:10.20944/preprints201608.0206.v2

37. Lazaro, A.; Girbau, D.; Villarino, R. Techniques for Clutter Suppression in the Presence of Body Movements during the Detection of Respiratory Activity through UWB Radars. *Sensors* **2014**, 14, 2595–2618.
38. Li, C.; Lin, J. Random body movement cancellation in Doppler radar vital sign detection. *IEEE Trans. Microw. Theory Techn.* **2008**, 56, 3143–3152.